12th International Symposium on Turbulence and Shear Flow Phenomena (TSFP12)
Osaka, Japan, July 19–22, 2022

LINEAR AND NON-LINEAR DYNAMICS OF STREAK BREAKDOWN IN A HYPERSONIC BOUNDARY LAYER

Clément Caillaud
DFTC-2AT
Institut Pprime / CEA-CESTA
Chasseneuil du Poitou, France
clement.caillaud@isae-ensma.fr

Guillaume Lehnasch
DFTC-2AT
Institut Pprime - ENSMA
Chasseneuil du Poitou, France
guillaume.lehnasch@isae-ensma.fr

Peter Jordan
DFTC-2AT
Institut Pprime - CNRS
Chasseneuil du Poitou, France
peter.jordan@univ-poitiers.fr

Eduardo Martini
DFTC-2AT
Institut Pprime / CEA-CESTA
Chasseneuil du Poitou, France
eduardo.martini@univ-poitiers.fr

Eric Goncalves
DFTC-2AT
Institut Pprime / ENSMA
Chasseneuil du Poitou, France
eric.goncalves@ensma.fr

Ludovic Hallo
CESTA
CEA-DAM
Le Barp, France
ludovic.hallo@cea.fr

ABSTRACT

Hypersonic vehicles often present curved geometries and rough surfaces, directly affecting the boundary layer topology. An important feature of the boundary layer in such conditions is a system of streaks. These streaks induce a flow distortion and lead to a new set of unstable modes. We study the effect of this boundary layer modification using Direct Numerical Simulation (DNS) of a flow at $M_\infty = 6.0$ over a flat plate. Optimal disturbances of increasing amplitudes are used to design a set of three stationary base flows containing growing streaks. We then perform DNS and linearised DNS of these base flows subjected to white-noise forcing. The forcing leads to the emergence of an ensemble of modes, which we identify and track with a flow decomposition using SPOD and Floquet theory. The transition scenarios for the streaky flows are studied. Specifically, we observe the early dominance of low-frequency modes in contrast with the Blasius boundary layer and previous PSE studies where the second Mack mode was given as dominant. Finally for this specific case, we highlight the importance of taking into account broadband forcing to study the streaky baseflows in order to appropriately track the evolution of relevant unstable modes.

Introduction

The geometry of hypersonic vehicles often resembles a slender geometry starting with a blunt forebody to reduce the stagnation temperature at the nose-tip. It has been demonstrated by Stetson (1983) that the transition dynamics can be strongly related to this bluntness (curvature radius) and that for large bluntness, transient growth of streaks is an important ingredient in the transition process (Paredes *et al.*, 2017*a*). Additionally, to alleviate the substantial heat fluxes, the thermal protection systems of such vehicles are designed to be ablative, progressively inducing the appearance of distributed roughness on the walls. This significantly increases the complexity of the transition process through modal growth and mechanisms issued from the deformed base flow associated with the roughness (Schneider, 2008). This may result in steady streaks that arise due to the lift-up mechanism.

While the evolution and breakdown of the hypersonic boundary layer for selected modal instabilities have been well documented (Franko & Lele, 2013), the path to transition via non-modal mechanisms lacks a clear understanding at high velocities. Recent studies by Paredes *et al.* (2017*b*, 2019) have provided a description of the linear growth of selected modes supported by the streaky boundary layer using PSE analysis. These studies demonstrated the co-existence of modes destabilised by the streaks and the usual second mode (Mack modes) and presented an overview of the linear amplification of selected modes for increasing streak amplitudes. Specifically, at $M_\infty = 5.3$ on a sharp cone, the second Mack-modes family was found to dominate for streak amplitudes up to 40% of u_∞. At hypersonic speed, the aforementioned PSE study also demonstrates stabilising effect of streaks on the second Mack mode growth for streak amplitudes around 10% of u_∞. However, investigation of the different modes receptivities and non-linear effects has not been addressed. Therefore, to complete these previous studies, the current work aims at providing insight into the receptivity, growth and non-linear dynamics of instabilities on a streaky base flow.

This study is organised as follows. After having defined the specifics of the computational framework, the base flows and forcing are described. Then the obtained disturbance fields from the DNS and LDNS are discussed. We first present an analysis of the linearly dominant modes at the end of the domain. Then, we decompose the disturbance fields using Floquet-SPOD and discuss the unstable modes. Finally, we track the dominant modes within the DNS domain and discuss the dependence of the transition scenario on the streak amplitude.

Simulation framework

A Direct Numerical Simulation (DNS) code: `CurviCREAMS` has been developed and is used to analyse the linear and non-linear stages of the hypersonic boundary-layer transition. The code solves the compressible Navier-Stokes equations for a mixture of thermally perfect gases in gener-

alized coordinates. The governing equations are computed in a finite-difference framework using 8th-order schemes and an adaptive shock capturing methodology consistent with the curvilinear framework. Additionally, to compare the linear and non-linear dynamics of disturbances evolving in the boundary layer, a discrete linearization procedure is implemented to perform Linearised DNS (LDNS). The construction of the LDNS is done in the spirit of Fosas de Pando *et al.* (2012) and is described hereafter. Consider the discrete non-linear operator of the Navier-Stokes equations: $\mathcal{N}(\boldsymbol{q})$, for a set of initial and boundary conditions. The dynamical evolution of any state vector $\boldsymbol{q}(x,t)$ reads:

$$\frac{\partial \boldsymbol{q}}{\partial t} = \mathcal{N}(\boldsymbol{q}). \tag{1}$$

Considering that the DNS code can compute $\mathcal{N}(\boldsymbol{q})$ for any given $\boldsymbol{q}$, the tangent linear operator $\mathcal{L}$ at a fixed point $\boldsymbol{q}_0(x)$ can then be extracted from the non-linear code by a first-order approximation,

$$\mathcal{L}(\boldsymbol{q}_0)\boldsymbol{q}' = \frac{\mathcal{N}(\boldsymbol{q}_0+\varepsilon\boldsymbol{q}') - \mathcal{N}(\boldsymbol{q}_0)}{\varepsilon}, \tag{2}$$

with ε a small value. This yields the linear dynamics of a disturbance vector $\boldsymbol{q}'$ around $\boldsymbol{q}_0$:

$$\frac{\partial \boldsymbol{q}'}{\partial t} = \mathcal{L}(\boldsymbol{q}_0)\boldsymbol{q}'. \tag{3}$$

Then, depending on its form, the disturbance vector $\boldsymbol{q}'$ introduced in Eq. 2 can be used either to extract the jacobian matrix $\mathcal{L}$ for a global stability analysis or to compute the linear time evolution of a chosen disturbance around $\boldsymbol{q}_0$. The latter approach is employed here. Therefore, the linear problem is time marched using the same schemes and boundary conditions as the non-linear solver for the same computational cost, allowing rigorous comparisons between LDNS and DNS results.

Setup and base flows

We consider the spatial development of a boundary layer over an adiabatic flat plate at $M_\infty = 6.0$, $Re_{\delta^*} = 28000$ and $T_\infty = 273.15K$. This boundary layer is developed from self-similar profiles injected at the inlet, from which we take the displacement thickness δ^* as the reference length. The domain is of size $L_x \times L_y \times L_z = 350 \times 15 \times 4\lambda_S$, with λ_S the streaks spanwise wavelength. Accounting for the sponge zones, we use a grid of $N_x \times N_y \times N_z = 4130 \times 335 \times 300$. On this base flow, the streaks are generated by a volume of stationary forcing close to the inlet and centred at $x_f = 5.0$. This stationary forcing consists of optimal vortical disturbances obtained with a 1D locally parallel, spatial transient growth analysis for a base flow profile at $x = 5.0$. The spatial transient growth analysis is carried out at a frequency $f = 0.0$ for a range of increasing spanwise wavenumbers to find the most amplified disturbance at the end of the domain. We ensure that upstream-travelling modes are filtered out from the spectrum before computing the spatial transient growth (Jordan *et al.*, 2017). To obtain optimal disturbances, we seek to maximize the gain $G(x = 350)$ between an initial disturbance $\boldsymbol{q}_0$ and a final response $\boldsymbol{q}_f$, defined as follows, with the norm $||\bullet||_E$ taken as the compressible energy norm (Hanifi *et al.*, 1996).

$$G = \frac{||q_f||_E}{||q_0||_E} \tag{4}$$

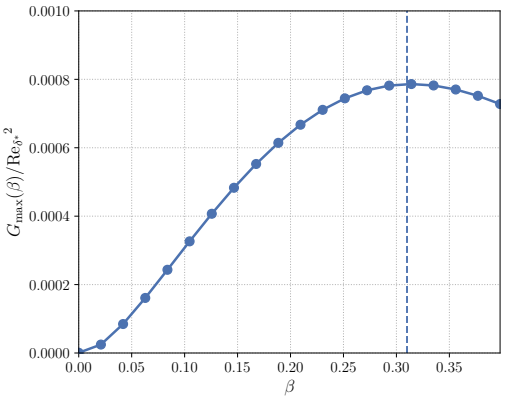

Figure 1: Rescaled transient growth gain G as a function of the spanwise wavenumber

This way, optimal vortices are found to have a spanwise wavenumber $\beta_S = 0.31$ similar to Andersson *et al.* (2001); Paredes *et al.* (2019) and the optimal disturbance gain evolution with $\beta = 2\pi/\lambda$ is given in Fig. 1. This spanwise wavelength serves as a parameter to define the spanwise extension of the DNS domain. We compute four streak periods ($z \in [0, 4\lambda_S]$) to account for the subharmonic secondary instability (Andersson *et al.*, 2001) and eventual instabilities of longer wavelength.

The linear optimal forcing is non-linearly propagated downstream with the DNS. We choose to study three cases of streak amplitudes $A_{su}(x) = \frac{1}{2}\left(\max_{y,z} u'(x) - \min_{x,y} u'(x)\right)$, named A1, A2 & A3. These are respectively constructed by increasing the initial optimal disturbance amplitude A_0. The associated streak amplitude evolution along the domain is given in Fig. 2a. These cases span the streak amplitudes studied by Paredes *et al.* (2019), with further emphasis on high-amplitude streaks (A3). We show the final shapes of the steady streaks $\bar{\boldsymbol{q}}$ modulating the base flow in Fig. 2b.

As we aim to understand which mode dominate, without selecting specific modes a priori, we introduce a white noise made of pressure disturbances in a volume centred at $x = 5.0$. We generate this noise following the procedure developed by Hader & Fasel (2019), slightly adapted to our case. We chose the forcing amplitude at $A_f = 5 \times 10^{-3}$ to trigger transition in the most sensitive case of the A3 streaks. Using this forcing, we perform, for each streak amplitude, DNS and LDNS simulations. The DNS allows us to get insights in the transition scenario, whereas the LDNS supports the study by capturing the linearly most amplified modes from the forcing.

For each simulation, we perform a time sampling of the solution to build a discrete state vector $\boldsymbol{q}$. We decompose this vector in frequency-wavenumber space to clarify the transition process. This analysis is supported by the results of a spatial 1D LST (Linear Stability Theory) analysis of a non-streaky boundary layer at the same flow conditions. We use this LST study to determine the frequency of the most amplified Mack mode in the domain. This mode, being the instability of highest frequency, guides us in selecting a proper Nyquist frequency. Obtaining a second Mack mode frequency of $f_M \approx 0.28$ close to the inlet, we use a Nyquist frequency of $f_s = 1.3$ to be able to capture this mode and its first harmonic. The sampling is performed over 1300 convective times $t_c = \delta^*/u_\infty$, resulting in 1300 snapshots of the flow evolution presented in next section.

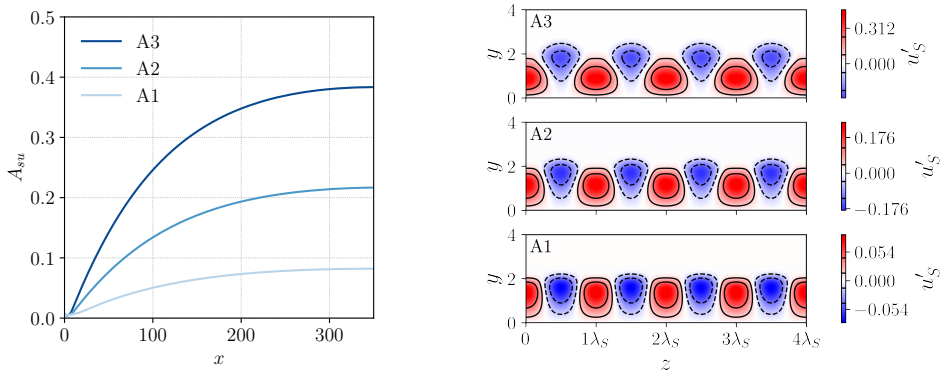

(a) Streaks amplitude A_{su}

(b) Streaks velocity disturbance u'.

Figure 2: Streaks amplitude evolution and final streaks shape at $x = 350$

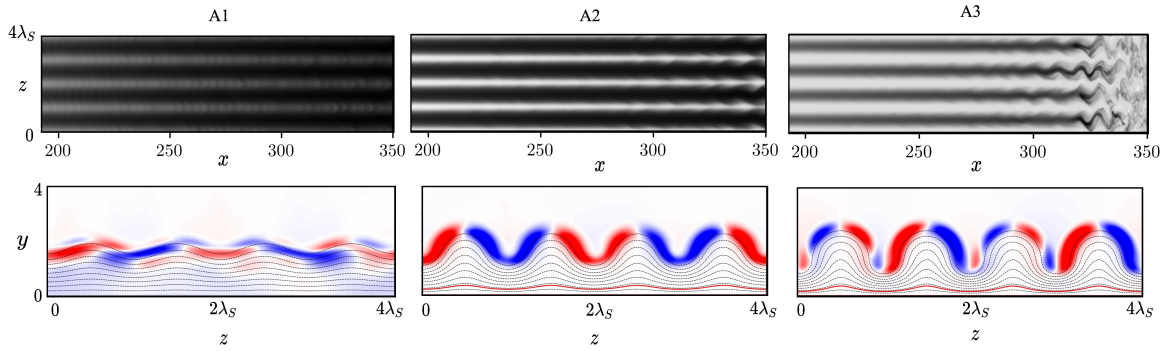

Figure 3: Top : normalised contours of axial velocity from the DNS at $y = 1.5\delta^*$. Bottom : associated LDNS axial disturbance velocity u' at $x = 350$. Dashed lines : contours of the base flow axial velocity.

Linear and non-linear disturbance fields

A first investigation is made with the DNS response to the white-noise forcing and the associated linear disturbances fields from the LDNS. These fields are presented in Fig. 3 for the DNS velocity field and the LDNS disturbances field obtained with Eq. 3. To help identify the growing modes, we also performed a 2D locally parallel LST at $x = 350$ for the streaky base flows. Out of conciseness, we only present the relevant unstable modes eigenfunctions on the left side of Fig. 5 for the first mode family (FM), second Mack mode family (MM) and streak modes family (SM). These modes serve as a reference for the identification of observable flow structures in Fig. 3.

The DNS velocity fields show various secondary structures as a function of streak amplitude. The A1 case shows a short streamwise wavelength in the velocity field that has no clear symmetry. This symmetry being defined as the symmetry of the axial disturbance velocity distribution about the low-speed streaks centerline. The associated LDNS disturbances look to comprise a superposition of many modes under this broadband forcing. For the A2 case, a spanwise motion of the streaks with a varicose organisation is noticed. Associated LDNS fields depict a marked anti-symmetric and subharmonic ($\lambda = 2\lambda_S$) disturbance distribution on the top of the boundary layer, suggesting the dominance of a single linear subharmonic and sinuous mode. Finally, the A3 case undergoes transition to turbulence before the end of the domain, following a sinuous motion of the streaks. The associated LDNS disturbance field at the end of the domain shows a superposition of at least two modes. One is spanwise harmonic ($\lambda = \lambda_S$) and the other is subharmonic, but both are anti-symmetric with respect to the low-speed streaks. This superposition suggests a competition mechanism between the modes triggered by the white-noise forcing that can be made clear by the decomposition of the solution fields.

Sparse L-periodic SPOD formulation

We decompose the disturbances vector $\boldsymbol{q}'_i$ for a case A_i in an optimal orthogonal basis using SPOD (Schmidt & Colonius, 2020). We point out that some special care should be given to the decomposition in our case. Considering the absence of an homogeneous direction in z for our base flow (i.e. $\partial\bar{\boldsymbol{q}}/\partial z \neq 0$), the usual decomposition into single spanwise modes to reduce the size of the problem cannot be performed. Nonetheless, given the L-fold symmetry of the streak pattern in the z-direction, with $L = 4$ here, we can make use of the Floquet theory to reduce the size of the analysis. Hence, the spanwise direction of $\boldsymbol{q}$ can be decomposed in three Floquet components for the $\lambda = [\lambda_S, 4\lambda_S, 2\lambda_S]$ spanwise periodic modes given respective Floquet exponents $M = [0, 1, 2]$, which respectively refers to harmonic, 4-streaks and subharmonic spanwise periodicity. Using the spanwise Fourier transform ($\tilde{\bullet}$), we obtain a complete basis of spanwise wavenumbers indexed by l for each Floquet exponent M,

$$\mathbf{q}'(x,y,z) = \sum_M \sum_l \tilde{\mathbf{q}}'_{M-Ll}(x,y) e^{i(M-Ll)z}. \qquad (5)$$

Following initial work on the SPOD formulation using Floquet theory by Rigas *et al.* (2019), where the use of spanwise-modes sparsity was not made to reduce the SPOD problem

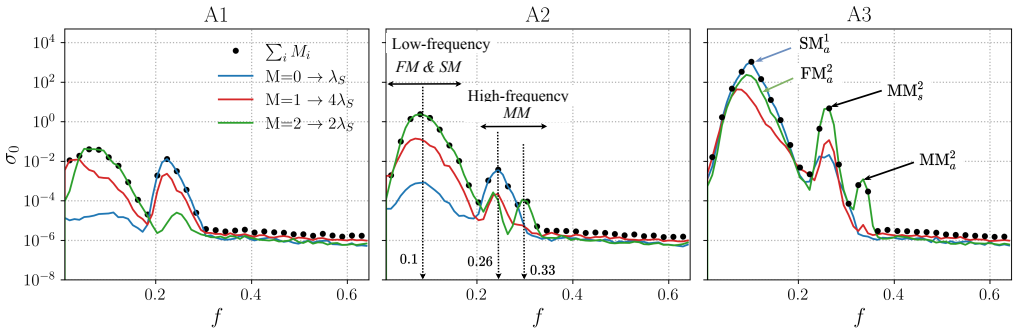

Figure 4: First SPOD eigenvalue energy at $x = 350$. Black : full spanwise modes base. Colors : spectrum by Floquet exponent. Blue : harmonic ; green : subharmonic ; red : 4-streaks spanwise periodicity.

size. We devise a complete development in the frequency-wavenumber domain to reduce the SPOD cost by only using relevant spanwise wavenumbers with respect to the streak periodicity considered. These developments are summarised in what follows.

We start with the usual cross-spectral density formulation $\mathbf{S}_{\text{ff}}$, with $\hat{\boldsymbol{Q}}$ the blocks matrix whose columns are made of a selected frequency issued from the time Fourier transform of $\boldsymbol{q}'$, using blocks of size $N_{\text{fft}} = 128$. Noting the hermitian transpose $\hat{\boldsymbol{Q}}^H$ and the space metrics dV, we write :

$$\mathbf{S}_{\text{ff}} = \int_V \hat{\mathbf{Q}}^H \mathbf{W} \hat{\mathbf{Q}} \text{dV}. \tag{6}$$

$\mathbf{W}$ is the matrix form of the compressible energy norm, and it is a function of the non-homogenous base flow $\bar{\boldsymbol{q}}$. This inhomogeneity of the base flow is what complicates formulating the sparse SPOD, in contrast to the homogeneous case, where just the $\beta = 0.0$ component of the base flow can be used. Specifically, a sparse SPOD should only take the relevant spanwise modes associated with the particular streak periodicity considered (harmonic, subharmonic, ...) to alleviate the computational cost of decomposing the DNS database. Hence, starting by from Eq. 6 in frequency-space domain, both the matrices $\mathbf{W}$ and $\hat{\mathbf{Q}}$ in Eq. 6 have to be Fourier transformed in the z-direction and only the relevant modes retained. Therefore, with $(\tilde{\bullet})$ the Fourier transform in z, and using the property of the Fourier transform, we can write the sparse expression of S_{ff} for a non-homogenous base flow within the Floquet framework,

$$\begin{aligned} \mathbf{S}_{\text{ff}} &= \int_V \tilde{\hat{\mathbf{Q}}}^H \widetilde{\mathbf{W}\hat{\mathbf{Q}}} \text{dV}, \\ &= \int_V \tilde{\hat{\mathbf{Q}}}^H \left(\tilde{\mathbf{W}} * \tilde{\hat{\mathbf{Q}}} \right) \text{dV}, \end{aligned} \tag{7}$$

with $(*)$ the convolution operator in the transformed direction. Using Eq. 7, we obtain a physically meaningful formulation of $\mathbf{S}_{\text{ff}}$ now in the frequency-wavenumber domain for non-homogeneous base flows. In the initial formulation of Rigas *et al.* (2019), the database is first Fourier transformed in z to filter only the relevant spanwise modes, then Fourier transformed back in space to perform the SPOD in the physical domain. Our formulation allows us to take full advantage of the Floquet decomposition of $\boldsymbol{q}'$ by using only a few relevant wavenumbers and keeping the SPOD analysis in wavenumber domain with significant computational savings. Finally, Eq. 7 leads to a cost reduction by a factor L to the SPOD computation.

LDNS spectra at x=350

Using the framework developed above, we compute the SPOD of $\boldsymbol{q}'$ for the LDNS at $x = 350$. We give in Fig. 4 an overview of the energy spectrum of the first eigenvalue σ_0 of the SPOD along with identified eigenfunctions in Fig. 5, the notations are defined below. A white noise forcing of identical amplitude for all streak cases was used. By looking at the black markers, summing all Floquet components in the z-direction, we notice at first sight a strong increase in the amplitude levels reached by the most amplified instabilities as A_{su} increases, showing how increasing the streak amplitude considerably amplify the linear growth mechanisms. Additionally, we notice a separation between low-frequency ($f \approx 0.1$) and high-frequency modes ($f > 0.22$). Using the 2D-LST results mentioned above, we identified the modes at $f = 0.1$ to belong to the first mode family (FM) and streak-modes family (SM), whereas the modes at $f > 0.22$ were identified to belong to the second Mack-mode family (MM). Specifically, for the high-frequency content, we notice the progressive separation of the high-frequency peak in the A1 case into two peaks of frequencies $f \approx 0.25$ and $f \approx 0.32$ for cases A2 & A3. This frequency separation has not been observed before and reveals two subfamilies of the Mack mode, which we shall describe later as being symmetric/varicose (MM_s) and anti-symmetric/sinuous (MM_a) Mack modes. To further help the detailed interpretation of these spectra in what follows, we make use of the convention $(\bullet)^k$ for modes of wavelength $\lambda = k\lambda_S$. E.g. MM_s^2 is the subharmonic sinuous second Mack-Mode as depicted in Fig. 5e.

Whereas for the A1 case, the low and high-frequency peaks are of a similar order of magnitude, with increasing streak amplitude (case A2 & A3), the low-frequency mode dominates: increasing the streak amplitude thus enhances the linear growth mechanism associated with the first mode. The strong amplification of the low-frequency content contrasts with the PSE results of Paredes *et al.* (2019) at similar values of Mach number and streak amplitude, where the introduced Mack mode was found to dominate. This difference underlines the importance of accounting for the receptivity process in the analysis of the transition on such distorted boundary layers.

Going further in the interpretation of the LDNS spectra, we look at the coloured lines of Fig. 4 representing the Floquet decomposition of the SPOD energy spectrum of the full spanwise base depicted in black, using Eq. 7. The blue, green and red curves give the frequency energy spectrum of respectively, harmonic ($\lambda = \lambda_S$), subharmonic ($\lambda = 2\lambda_S$) and four-streaks modes ($\lambda = 4\lambda_S$). Each energy peak of the coloured curves has been identified as an independent 2D-LST mode. This decomposition highlights a rich modal content for the streaky-

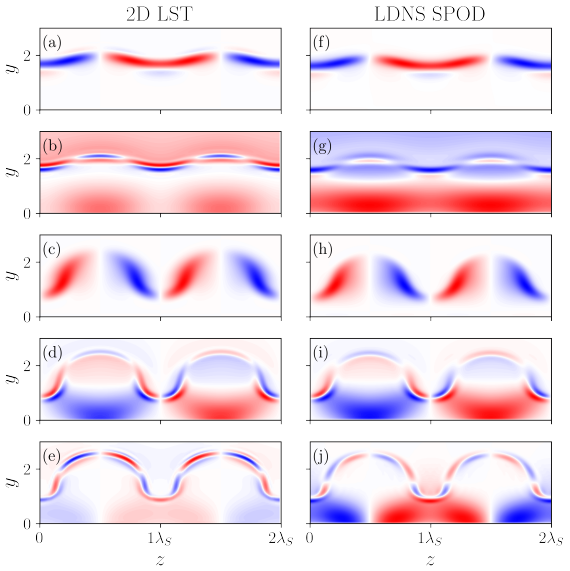

Figure 5: Comparison of LST-2D (left) and SPOD (right) eigenfunctions at $x = 350$. Normalised contours of the real part of the axial velocity disturbance. Modes shape for A2 are not shown as they are the continuation of A1. (a) : A1 $f = 0.08, \mathrm{FM}_a^2$; (b) : A1 $f = 0.26, \mathrm{MM}_s^1$; (c) : A3 $f = 0.09, \mathrm{SM}_a^1$; (d) : A3 $f = 0.26, \mathrm{MM}_s^2$; (e) : A3 $f = 0.33, \mathrm{MM}_a^2$

boundary layers.

The modes FM_a^2 at $f = 0.08$ (Fig. 5a) and MM_s^1 (Fig. 5b) drive the dynamics of case A1. As the streak amplitude increases, for case A2, the low-frequency mode FM_a^2 becomes dominant. Concurrently, we note in Fig. 4 a decrease of 70% in the amplitude of the mode MM_s^1, suggesting a stabilizing effect also noted in Paredes *et al.* (2019). We also note the emergence of the secondary peak at $f = 0.33$ for the subharmonic component MM_a^2 (Fig. 5e). Finally, for case A3, the low-frequency mode that has here become dominant switches to a harmonic spanwise periodicity (SM_a^1) (Fig. 5c). Concurrently, the decaying harmonic Mack mode switches to a subharmonic Mack mode (MM_s^2) (Fig. 5d), strongly amplified compared to cases A1 & A2. This amplification suggests now a destabilising effect of the high amplitude streaks.

Non-linear dynamics

Having assessed the most amplified instabilities originating from the white noise forcing. We compare and track these identified modes in the non-linear simulation. Using Eq. 7, the growth of the main modes retained from Fig. 4 can be followed in Fig. 6 for cases A1, A2 & A3. For further comparison, we also compute the LDNS of the white noise forcing of a Blasius boundary layer, i.e. without streaks, at exactly the same flow conditions. We add the most amplified first mode and Mack mode issued from this non-streaky LDNS to the figures to quantify the streaks effect. Hence Fig. 6 contains the DNS and LDNS results for streaky base flows with respectively thick and dashed lines, and it also contains LDNS results for the non-streaky base flow, shown as thin dotted lines with markers. As cases A1 & A2 follow a similar trend, with increased dominance of FM_a^2, the A3 case reveals more intricate non-linear dynamics requiring the tracking of additional modes.

The DNS of case A1 does not reach turbulence by the end of the domain. Both amplified DNS modes follow the amplification rate of their LDNS counterpart, especially the MM_s^1 mode closely follows the LDNS up to $x > 200$. We can notice that the receptivity in the non-linear regime shows a slight discrepancy with a delayed growth of the low-frequency mode with respect to the LDNS. Suggesting that some non-linear receptivity mechanism might be at play. Comparing these observations to the non-streaky LDNS, we note an overall delaying effect of the streaks on the linear receptivity and growth of these unstable modes. We also remark, as noted by Paredes *et al.* (2019), a reduction in the Mack mode amplification rate, confirming the stabilising effect at this low streak amplitude of $A_s u \approx 0.1$. On the other hand, the first mode shows an increased amplification.

The dynamics of case A2 are driven by the FM_a^2 mode on the second half of the domain. This mode has a strong amplification rate compared to the non-streaky case, showing increased instability. On the other hand, the Mack-mode MM_s^1 shows a fast initial growth, followed by a stabilisation. A second interesting feature is a discrepancy between the initial growth of the DNS and LDNS Mack modes. The former starts to grow strongly around $x = 80$ where the LDNS mode amplification shows a considerable delay. This early non-linear growth suggests the presence of a non-linear receptivity mechanism for the MM_s^1 mode. Furthermore, after the strong initial growth, the Mack mode observes a damping resulting in an amplitude decay from $x = 150$. Although delayed, similar behaviour is observed for the LDNS. Then, the MM_s^1 from the DNS shows an almost constant growth rate. Its LDNS counterpart shows a stronger growth at $x = 200$ up to $x = 280$ where its starts getting damped again. This discrepancy could be explained by the non-linear base-flow modification due to the varicose motion observable in Fig. 3 at $x \approx 280$, supporting the instability of the DNS MM_s^1 mode

Finally, we investigate the transitional scenario of case A3. At first sight, the non-linear dynamics seem to be driven by two low-frequency modes, which are the subharmonic FM_a^2 and the harmonic SM_a^1 modes. This latter mode is noted as a streak mode because it hase be identified to unstable only for higher streak amplitude by 2D-LST. The FM_a^2 mode has an early receptivity and a constant growth throughout the domain, while the SM_a^1 mode starts being linearly unstable only after $x = 120$ but quickly outgrows the FM_a^2 mode as the streaks amplitude increases. From this spectrum, it seems that both modes leads to the onset of turbulence around $x = 300$. However, looking at Fig. 3 we observe an harmonic sinuous motion related to mode SM_a^1 symmetry, favouring the hypothesis of the final stages of transition being dominated by the strong growth of this latter mode for this specific case. Although, this result does not rule out the possibility of a transition driven by the earlier amplification of the subharmonic instability in a noisier environment. As for the high-frequency content, we now observe the strong amplification of the MM_s^2 mode. This amplification exceeds the Mack modes growths of cases A1 & A2, suggesting an increased instability of the Mack modes for large streaks amplitude.

These combined observations for all three cases reveal the strong effect of the streaks distortion on the boundary layer receptivity and stability. The main result here is the effect of the streaks on the Mack-mode receptivity and the first mode amplification. It shows that even for low streaks amplitude, the dominance of the second Mack mode observed for the Blasius case is no longer verified. Furthermore, these results suggest that the family of the low-frequency modes is actually dominant at $M_\infty = 6.0$ for all the observed streaks amplitude here.

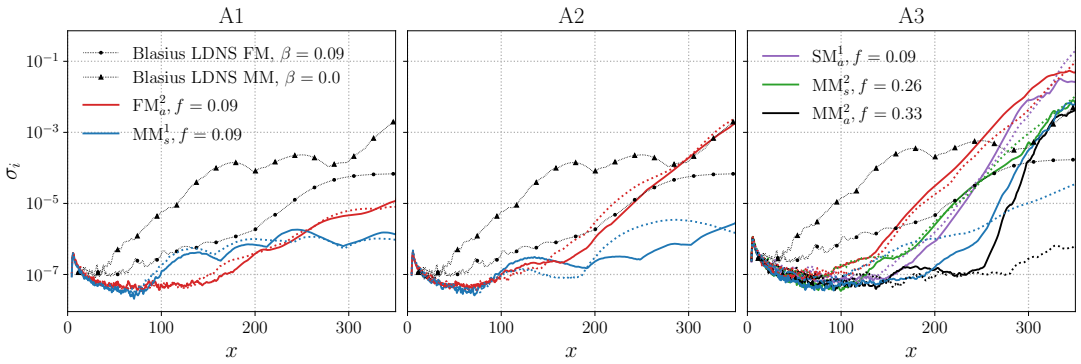

Figure 6: Non linear evolution of the main SPOD modes energy (full), compared to the rescaled LDNS dynamics (dotted).

Conclusion

In this study, we have investigated the effects of steady streaks on the boundary layer receptivity, stability and transition. In order to get a further understanding of these effects, we devised a DNS framework to study the linear and non-linear dynamics of disturbances triggered by white noise. We apply this forcing on three steady base flows consisting of growing optimal streaks of three different amplitudes spanning previously studied amplitudes from the PSE analysis of Paredes *et al.* (2019) at a similar Mach number.

To decompose the dynamics in time and space, we developed an SPOD formulation using Floquet theory, which allows us to split the growing modes into different families according to their periodicity with respect to the streaks. This method allows us to capture the emergence of a larger number of distinct modes in the streaky flow compared to the Blasius boundary layer. By comparing the linear growth of these modes to previous linear analyses, we highlight the role of the forcing and receptivity in the evolution of the modes. We show a strong amplification and dominance of low-frequency modes for all streak amplitude considered in contrast with the previous PSE results.

Going further in the analysis by tracking the non-linear evolution of the most amplified modes, the DNS shows the various effects of the streaks on the mode receptivity and growth compared to the streaky-linear and the non-streaky, Blasius boundary layers. In short, the Mack modes are mainly damped by the streaks and their receptivity is also affected. Also, the low-frequency modes of subharmonic spanwise periodicity dominate at low amplitude, whereas the strong amplification of the harmonic component is leading to turbulence at high amplitude. This set of results serves as a first estimation of natural transition dynamics in a streaky boundary layer. Finally, this study underlines the sensitivity of the receptivity, modal growth and non-linear stages of transition process to slight changes in the boundary layer topology. Further analysis will now be necessary to understand which underlying physical mechanisms drive these changes in the flow dynamics.

Acknowledgements

This work is part of the project TRANSITION supported by Région Nouvelle Aquitaine under grant 2018-1R10220. Additionally, this work was granted access to the HPC ressources of IDRIS under the allocations 2020-A0092A10868 and 2021-A0112A10868 made by GENCI.

REFERENCES

Andersson, Paul, Brandt, Luca, Bottaro, Alessandro & Henningson, Dan S. 2001 On the breakdown of boundary layer streaks. *Journal of Fluid Mechanics* **428**, 29–60.

Franko, Kenneth J. & Lele, Sanjiva K. 2013 Breakdown mechanisms and heat transfer overshoot in hypersonic zero pressure gradient boundary layers. *Journal of Fluid Mechanics* **730**, 491–532.

Hader, Christoph & Fasel, Hermann F. 2019 Direct numerical simulations of hypersonic boundary-layer transition for a flared cone: fundamental breakdown. *Journal of Fluid Mechanics* **869**, 341–384.

Hanifi, Ardeshir, Schmid, Peter J. & Henningson, Dan S. 1996 Transient growth in compressible boundary layer flow. *Physics of Fluids* **8** (3), 826–837.

Jordan, Peter, Zhang, Mengqi, Lehnasch, Guillaume & Cavalieri, André V. 2017 Modal and non-modal linear wavepacket dynamics in turbulent jets. In *23rd AIAA/CEAS Aeroacoustics Conference*. Denver, Colorado: American Institute of Aeronautics and Astronautics.

Fosas de Pando, Miguel, Sipp, Denis & Schmid, Peter J. 2012 Efficient evaluation of the direct and adjoint linearized dynamics from compressible flow solvers. *Journal of Computational Physics* **231** (23), 7739–7755.

Paredes, Pedro, Choudhari, Meelan M. & Li, Fei 2017*a* Blunt-body paradox and transient growth on a hypersonic spherical forebody. *Physical Review Fluids* **2** (5), 053903.

Paredes, Pedro, Choudhari, Meelan M. & Li, Fei 2017*b* Instability wave–streak interactions in a supersonic boundary layer. *Journal of Fluid Mechanics* **831**, 524–553.

Paredes, Pedro, Choudhari, Meelan M. & Li, Fei 2019 Instability wave–streak interactions in a high Mach number boundary layer at flight conditions. *Journal of Fluid Mechanics* **858**, 474–499.

Rigas, Georgios, Pickering, Ethan M., Schmidt, Oliver T., Nogueira, Petrônio A., Cavalieri, André V., Brès, Guillaume A. & Colonius, Tim 2019 Streaks and coherent structures in jets from round and serrated nozzles. In *25th AIAA/CEAS Aeroacoustics Conference*. Delft, The Netherlands: American Institute of Aeronautics and Astronautics.

Schmidt, Oliver T. & Colonius, Tim 2020 Guide to Spectral Proper Orthogonal Decomposition. *AIAA Journal* **58** (3), 1023–1033.

Schneider, Steven P. 2008 Effects of Roughness on Hypersonic Boundary-Layer Transition. *Journal of Spacecraft and Rockets* **45** (2), 193–209.

Stetson, K. 1983 Nosetip bluntness effects on cone frustum boundary layer transition in hypersonic flow. In *16th Fluid and Plasmadynamics Conference*. Danvers,MA,U.S.A.: American Institute of Aeronautics and Astronautics.